APPLIED ORGANOMETALLIC CHEMISTRY, VOL. 11, 107–127 (1997)

REVIEW

Novel, Organically Doped, Sol–Gel-Derived Materials for Photonics: Multiphasic Nanostructured Composite Monoliths and Optical Fibers

Raz Gvishi, Upvan Narang, Gary Ruland, Deepak N. Kumar and Paras N. Prasad*
Photonics Research Laboratory, Department of Chemistry, State University of New York at Buffalo, Buffalo, NY 14260-3000, USA

Sol–gel-processed organic–inorganic hybrid materials combine the merits of inorganic glass and organic molecules, and are therefore a class of materials with good potential for photonics. In this review, two approaches which have shown promising results for producing useful materials for photonics are described: (i) a novel way to fabricate organically doped, multiphasic nanostructured composite monoliths and (ii) a method of fabrication of organically doped, sol–gel-derived optical fibers. For each approach, the preparation process is presented, together with selected applications such as multidye solid-state tunable laser, multiphasic optical power limiter, a micron-scale chemical-sensing and biosensing fibers and solid-state dye-doped fiber lasers. © 1997 by John Wiley & Sons Ltd.

Keywords: sol–gel; composite glass; fiber; dye laser; optical power limiter; nonlinear optics; multiphasic nanostructured composites

CONTENTS

1 INTRODUCTION

Photonics is emerging as a multidisciplinary frontier of science and technology that has captured great interest among scientists and engineers around the world.[1–4] Much of the present interest arises because of the applicability of photonics to current and future information- and image-processing technologies. Photonics is analogous to electronics in that it describes the technology by which photons (instead of electrons) are used to acquire, store,

* Author to whom correspondence should be sent.

CCC 0268–2605/97/020107–21

Received 4 October 1995
Accepted 17 March 1996

transmit and process information. Lasing, waveguiding emission, the ability to alter the frequency or colour of light, and the ability to amplify, switch or alter the transmission characteristics through a medium of one source of light with another, are some potential useful linear and nonlinear optical processes which provide key functions for photonics.

The realization of this advanced technology rests on the development of multifunctional materials which simultaneously satisfy many functional requirements.[5, 6] The progress during the last decade in the design of organic systems makes it possible to prepare new materials with promising lasing and nonlinear optical properties.[7, 8] Molecules and polymers with π-conjugated electron systems have been the most widely studied organic optically active materials and show a promising performance. A major effort has been centered on introducing the optically active organic materials into a photostable medium such as a glass matrix, allowing their use as building blocks for photonic devices. Although organic polymers are commonly used as a solid matrix for hosting organic molecules,[9] they generally suffer from lack of photostability and optical quality.[10–13] This provides motivation for the successful introduction of active organic molecules into a more photostable inorganic glass. However, the introduction of an organic dye into an organic glass is not possible using the traditional glass-processing techniques because of the high processing temperatures (>800 °C) involved. In the early 1980s, when the sol–gel process became a popular method for preparing glasses at room temperature, Avnir and Reisfeld demonstrated for the first time that an organic dye can be doped within an inorganic glass.[14] Since then, many groups around the world have introduced organic materials into a variety of inorganic matrices via the sol–gel process. Sol–gel processed materials have been used in areas ranging from novel solid-state lasers to platforms for chemical sensors and biosensors.[15–22] Also, the sol–gel technique has been used to fabricate nonlinear optically active composites for applications in optical telecommunications.[5] Organically modified and sol–gel-processed materials have also been shown to exhibit excellent nonlinear optical $\chi^{(2)}$ and $\chi^{(3)}$ properties.[23]

In order to perform photonics functions, high optical quality and efficient fluorescent or nonlinear optical materials are needed. The best optical medium is an inorganic glass, such as silica. However, the active optical response of inorganic glasses is extremely weak. Inorganic crystals, which exhibit high optical response are expensive and difficult to fabricate. On the other hand, optically active organic polymers do not exhibit the optical quality of an inorganic glass and suffer from a lack of photostability. Sol–gel-processed inorganic matrices which can incorporate active organic molecules with high photostability are expected to be an attractive solution to this problem. Also, sol–gel-processed glasses offer an exciting potential as host matrices for doping optically active organic molecules.

To date, there are few sol–gel-derived materials which meet the materials quality required for fabricating devices. One of the major problems has been to produce useful bulk materials, free of cracks, and with controlled doping (organic and inorganic) at the nanoscale level. Another problem has been the fabrication of an optical fiber with active species incorporated within it. Moreover, photonics has a special requirement for devices which can operate over a wide range of wavelengths and exhibit more than one optical functionality.

In this report, two sol–gel-processed approaches which have shown promising results in producing useful materials for photonics are reviewed: (1) multiphasic nanostructured composites, which combine the merits of inorganic glass and an organic polymer;[24–26] and (2) optical fibers with active molecules incorporated within the fiber matrix, dispersed homogeneously, for sensing or lasing applications.[27, 28] For both approaches, the preparation process and selected applications based on past and current results obtained primarily in our own laboratory are described.

2 SOL–GEL-PROCESSED MATERIALS

2.1 Introduction; sol–gel process

Sol–gel processing involves the hydrolysis of a metal alkoxide, followed by a cascade of condensation and polycondensation reactions. More detailed information pertaining to the chemistry of sol–gel processing can be found in several recent books and review articles.[29–34] Briefly, the hydrolysis and polycondensation of a metal

alkoxide dissolved in a proper solvent yields a colloidal suspension of the reaction product called a 'sol'. The sol undergoes a transition to a soft porous mass, a wet gel, which eventually becomes a solid porous aggregate of extremely small particles known as the 'xerogel'. If the xerogel contains enough strong metal–oxygen bonds such as Si—O, it can be converted into a monolithic glass consisting of a random three-dimensional network of bonds by simply sintering or hot-pressing at a temperature well below the liquidus temperature of the system.[35] The low-temperature processing conditions associated with the sol–gel process makes it possible to encapsulate organic species within a sol–gel-derived inorganic matrix without decomposing the organic molecule.

The most commonly used precursor materials used for silica sol formation are tetramethoxysilane (TMOS) and tetraethoxysilane (TEOS). The basic reactions of a sol–gel system undergoing concurrent hydrolysis and condensation are:

$$n\mathrm{Si(OR)_4} + 4n\mathrm{H_2O} \leftrightarrow n\mathrm{Si(OHO_4} + 4n\mathrm{ROH} \quad [1]$$

$$n\mathrm{Si(OH)_4} \rightarrow n\mathrm{SiO_2} + 2n\mathrm{H_2O} \quad [2]$$

A promising class of sol–gel-derived materials comprises organic/inorganic hybrid materials which combine the merits of an inorganic glass and an organic polymer. A novel way to prepare nanocomposite monoliths of high optical quality and with desirable mechanical behavior is by forming first a glass monolith with controlled porosity by the sol–gel process, as a rigid matrix. Then, an organic monomer is diffused into the open pores and polymerized inside. This method was pioneered by Mackenzie and co-workers;[10] fabrication of a glass monolith with controlled porosity was extensively studied by Hench *et al*.[36]

2.2 Composite glasses

The chemical preparation of an inorganic oxide such as silica under carefully controlled condition produces pores of nanoscale size which can be impregnated with an organic phase, resulting in a composite glass.[10–12, 36–38] The silica skeleton of the composite glass is prepared by a two-step hydrolysis process. First, an acid catalyst is used which leads to a high degree of cross-linkage. Then a base catalyst is used which leads to fast gelation. The resulting product is a highly porous monolith with small pores. Using a moderate heat treatment, porous glass is obtained. By impregnating an organic monomer (such as methyl methacrylate), which diffuses into the pores, and by polymerizing it *in situ*, the composite glass can be obtained. After a polishing procedure, a material with high optical quality and mechanical strength results. A preparation protocol for composite glasses is described in more detail as follows.

The composite glass was fabricated following the method described by Gvishi *et al*.[37, 38] Highly porous silica-gel bulk glasses were prepared by a two-step hydrolytic sol–gel process,[10] starting from a precursor solution which contained tetraethoxysilane (TEOS) and ethanol in the molar ratio 1 : 4. After one hour of pre-hydrolysis, water (molar ratio 4) and HNO_3 (molar ratio 0.06) were added to complete the hydrolysis. This was followed by the addition of HF (molar ratio 0.8) to achieve fast gelation. The solution was then covered with a lid with small orifices to allow the solvents to escape and kept for aging at 40 °C for 1–3 weeks. The bulk gels were then dried by slow heating (60 °C h^{-1}) from room temperature to 500 °C. These glasses had an initial surface area of about 850 $m^2\,g^{-1}$, a pore volume of 68% and an average pore size of 46 Å (measured using nitrogen adsorption isotherms and calculated by the BET method).[38, 39] These bulk glasses (dimensions 10 mm × 5 mm × 1–5 mm) were immersed in the methyl methacrylate (MMA) monomer solution for 10–15 min. The MMA solution diffused into the sol–gel-derived glass pores and was polymerized therein using benzoylperoxide (2%) as the initiator. The MMA-doped bulk glasses were then re-immersed in an MMA–dye solution, which at this stage was initiated for full polymerization with benzoyl peroxide (0.5%), and kept in a sealed container at 40 °C until the polymerization process was completed (a few days). After completion of the polymerization process, the samples were withdrawn, cleaned with chloroform, and polished to obtain parallelpiped slabs with clear, smooth surfaces. The polishing method consisted of the following stages: pre-polishing on a SiC paper (300 and 600 grit in gradual steps) using deionized water as the lubricant, followed by fine polishing on cloth using 1 and 0.25 μm grade diamond pastes as abrasives. A commercial water-based fluid (Buehler) was used as the lubricant. The polishing procedures were performed manually on a Buehler polishing wheel. The final composite

glass contains 32 vol% silica and 68 vol% PMMA and is totally inactive for adsorbing nitrogen.[12] The observed density (1.447 g cm^{-3}) and refractive index (1.472) are in good agreement with the expected values from the average microproperties of the separate phases.[21] These composite glass exhibit excellent transmission over most of the visible range since the size of the domains is on a nanometer scale.

There are several methods of doping active molecules, depending on their nature, in the composite glass. Inorganic species such as Er^{3+} are doped through the precursor solution. Organic molecules can be impregnated in the interface phase through solution, melt or vapor infiltration, and in the organic polymer phase through the monomer solution. This approach yields the possibility of fabricating a composite glass which consists of many phases; but the phase separation is on a nanometer scale. Using this method, it is possible to dope two (or more) different optically responsive materials, each of which will be in different phases of the matrix (silica phase, PMMA phase or interfacial phase), to make multifunctional bulk materials for photonics.[24–26] The concept of a multiphasic nanostructured composite will be discussed in more detail in the next section.

2.3 Multiphasic nanostructured composites

Composite glasses prepared via the sol–gel technique are of high optical quality[12] and large monolithic bulk forms can be made for various photonic functions, such as lasing,[21, 22, 40] optical power limitation,[41, 42] nonlinear optical response[43] etc. An advanced approach is to form multiphasic nanostructured composites.[24–26] By a multistep impregnation method, one can dope two (or more) different optically responsive materials, each of which resides in different phases of the matrix (the silica phase, the organic polymer phase and the interfacial phase). For example, in the silica phase, any species that can survive the thermal treatment can be doped. Examples are inorganic species, such as rare-earth ions, which exhibit amplifying performance (Er^{3+} Eu^{3+}). In the interfacial phase, inorganic or organic species can be doped. Examples are semiconductors such as ZnS and CdS that—due to the nanoscale size of the pores—can be quantum dots with promising nonlinear properties, C_{60} (which exhibits a power limiting effect due to reverse saturable absorption) and other $\chi^{(3)}$ materials.[24, 25] Ionic dyes which exhibit strong two-photon absorption and induced up-conversion lasing can also be incorporated in the interfacial phase.[44–46] The only limitation for doping in the interfacial phase is that the dopant is not soluble in the monomer liquid (such as methyl metacrylate) that will be polymerized *in situ*. In the polymer phase, one can dope laser dyes and $\chi^{(3)}$ organic chromophores.[26, 43]

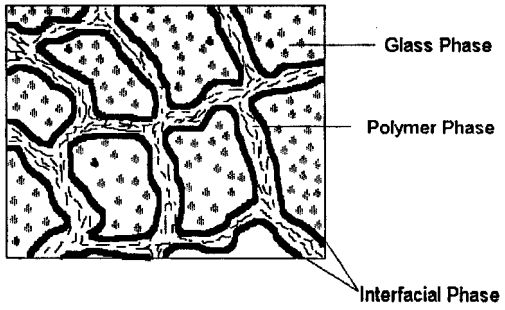

Figure 1 A simplified schematic representation of the multiphasic composite glass.

The basic design of the multiphasic nanostructured composite is explained by Fig. 1. In the inorganic glass phase (phase no. 1) itself, we can dope inorganic species. Then the pores can be impregnated by organic functional molecules through solution, or by using a melt or vapor-phase infiltration. After driving the solvent out, the organic molecules form a phase (phase no. 2) on the surface of the pores. Finally, the pores are filled with a polymerizable liquid, such as methyl methacrylate, which polymerizes in the pores to seal them. Another organic species, exhibiting a different functionality, can also be introduced in the polymer phase (phase no. 3), thus producing a solid solution of it. The monoliths prepared by this approach are of high optical quality and suitable for many applications in photonics.

We demonstrated the usefulness of a multiphasic composite through the fabrication of two specific devices: a multidye solid-state tunable laser[26] and a multiphasic optical power limiter.[24, 25] The multidye solid-state tunable laser consisted of a new laser dye, an aminostyrylpyridinium derivative (ASPD)[44–46] which resides in the interfacial phase, and Rhodamine-6G (R6G) which resides in the polymer phase. Figure 2 presents the fluorescence emission of a multiphasic composite glass containing both dyes. For reference the fluorescence emission spectra of two composite glasses containing each dye

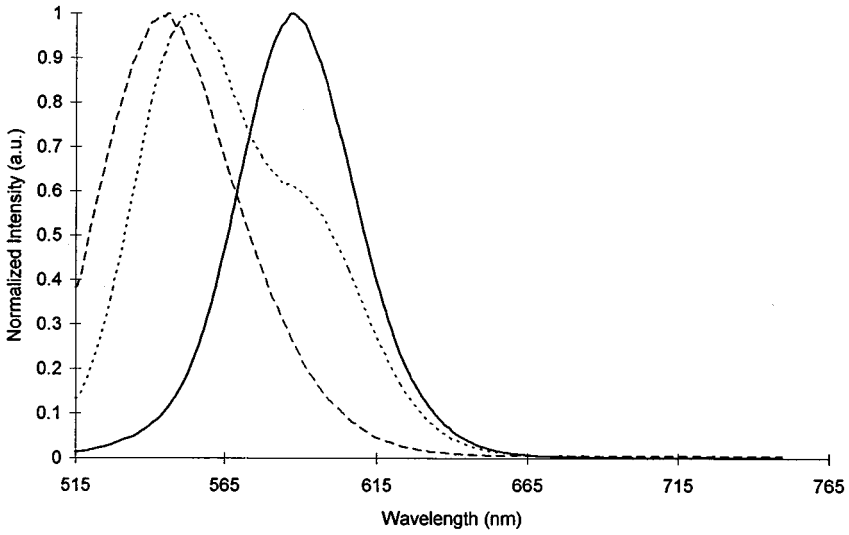

Figure 2 Fluorescence emission of Rhodamine-6G composite glass (broken curve), ASPI composite glass (solid curve) and the composite glass containing both dyes (dotted curve).

separately are presented as well.[26] We observed emission from both dyes in the multiphasic composite glass with no significant quenching of emission from either dye. Tunable lasing was observed across the region of the individual dyes,[26] (an extended discussion of this application is presented in Section 3.1.). Figure 3 presents the absorption spectrum of a multiphasic nanostructured composite doped with C_{60} (buckminsterfullerene) in the interfacial phase and a dye, bisbenzothiazole 3,4-didecyloxythiophene (BBTDOT), in the polymer phase.[24] Panel A shows a typical spectrum of BBTDOT in the composite glass.[37] Panel B presents a closer look at the red region, exhibiting a weak peak at 626 nm, which corresponds to the 0⟶0 transition of C_{60}.[47] Efficient optical power limiting was observed at two different wavelengths due to the

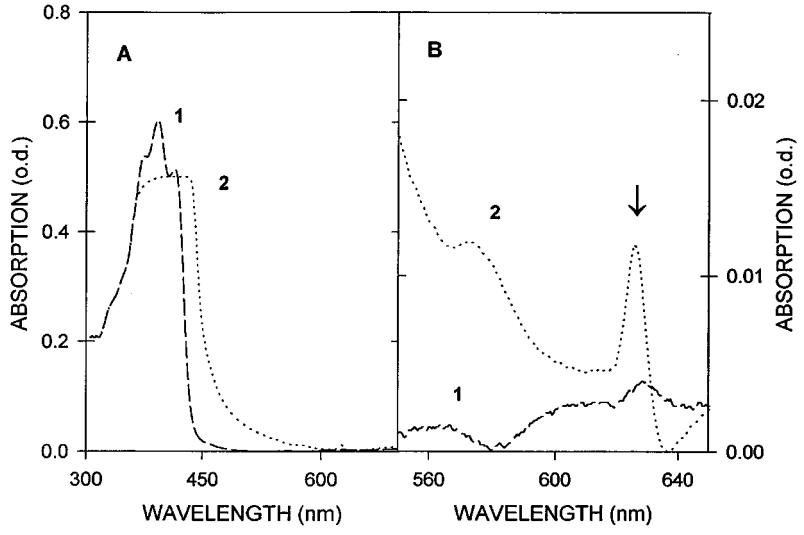

Figure 3 Absorption spectra of BBTDOT ($\sim 10^{-4}$ M) doped composite glass (curve 1—dashed line) and C_{60} (0.5% wt/wt) and BBTDOT ($\sim 5 \times 10^{-2}$ M) both doped in a multiphasic nanostructured composite glass (curve 2—dotted line). Part A: UV–visible absorption spectrum. Part B: a magnified spectrum of the red region. The arrow indicates the O⟶O transition of C_{60} which appears at 626 nm.

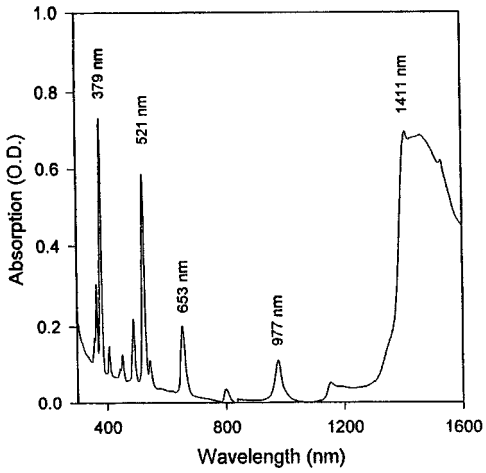

Figure 4 Absorption spectrum of Er^{3+}-doped porous sol–gel glass.

two different components[24] (an extended discussion of this application is presented in Section 3.2). Figure 4 shows the absorption spectrum of Er^{3+} doped in the silica phase. The typical absorption peaks of erbium are clearly seen as sharp peaks at 365, 379, 407, 452, 488, 521, 543, 653 and 977 nm; and there is a complex absorption band with peaks at 1411, 1463 and 1532 nm.

2.4 Microenvironment characterization

In order to achieve good optical performance from an active organic molecule doped within a composite glass, one requires an understanding of how the matrix affects the active molecule entrapped within. The local microenvironment can be probed using a solvent-sensitive probe.[19, 20] We used two spectroscopic methods:

(1) steady-state fluorescence: the Lippert expression gives a first approximation of the Stokes shift as a function of the solvent orientational polarizability;[55–58] and
(2) time-resolved fluorescence by deriving the excited-state decay kinetics using multi-frequency phase and modulation fluorimetry.[59, 60]

2.4.1 Steady-state fluorescence

To a first approximation, the Stokes shift is a function of the orientational polarizability and is given by the Lippert expression:[55]

$$\Delta\tilde{\nu} \equiv (\tilde{\nu}_a - \tilde{\nu}_e) = (\tilde{\nu}_a - \tilde{\nu}_e)_v + \frac{2(\mu^\star - \mu)^2 \Delta f}{hca^3} \quad [3]$$

where $\tilde{\nu}_a$ is the wavenumber of the absorption peak, $\tilde{\nu}_e$ is the wavenumber of the emission peak, $(\Delta\tilde{\nu})_v = (\tilde{\nu}_a - \tilde{\nu}_e)_v$ is the Stokes shift of the molecule in the vapor state. The orientational polarizability (Δf) is defined as $\Delta f = f(\varepsilon) - f(n)$,[61] where $f(\varepsilon) = (\varepsilon - 1)/(2\varepsilon + 1)$; $f(n) = (n^2 - 1)/(2n^2 + 1)$; ε is the low-frequency relative dielectric constant and n is the optical refractive index in the visible range; μ and $\mu^\star$ are the ground- and excited-state dipole moments, respectively; h is Planck's constant; c is the speed of light; and a is the characteristic dimension of the probe molecule.

The microenvironment experienced by the dye-doped multiphasic nanostructure composite was studied by fitting the observed Stokes shift of the dye in the multiphasic nanostructured composite to the Lippert plot obtained for the dye in liquid solutions. As examples two systems are shown;

(1) for 6-propionyl-2-(dimethylamino)naphthalene (PRODAN) which was impregnated in the glass initially via the methyl methacrylate monomer, and thus located in the polymer phase;[38]
(2) for *trans*-4-[*p*-(*N*-ethyl-*N*-hydroxyethylamino)styryl]-*N*-methylpyridinium tetraphenylborate/iodide (ASPD), which was impregnated in the glass initially via solution infiltration, and thus located in the interfacial phase.[44]

Figure 5 presents the Lippert plot [Stokes shifts (cm^{-1}) vs orientational polarizability (Δf)] for PRODAN in various liquid solvents (●) and solid matrices (□).[38,56] The observed values for absorption and emission maxima in various liquid solutions and in solid matrices, as well as the calculated Stokes shift, dielectric coefficients and refractive indices, are summarized in Table 1.[38] The numbers next to the data in Fig. 5 correspond to the numbers in Table 1, identifying the solvent used. In the PRODAN-doped composite glass, it would be expected that the observed Stokes shift would be the same as in PMMA, since the dye was impregnated in the glass matrix via methyl methacrylate monomers. However, by comparing the data for the composite glass with the observed Lippert plot for the solutions, one notices that the microenvironment

experienced by PRODAN is a combination of PMMA and sol–gel-like environments. In addition, the Stokes shifts in the solid matrices obey a similar dependence on Δf as is observed in the liquid solvents. Therefore, in the composite glass (which is a two-phase matrix), a microenvironment similar to the one expected from an average macroenvironment is observed.

Figure 6 shows the Lippert plot ([Stokes shifts (cm^{-1}) vs orientational polarizability (Δf)] for ASPD in various liquid solvents (●) and in solid matrices (□). The solid line represents the best fit for the data in liquid solvents.[44,64] The observed values in various liquid solutions and solid matrices of absorption and emission maxima, as well as the calculated Stokes shifts, dielectric coefficients and refractive indices, are summarized in Table 2.[44, 64] The numbers next to the data in Fig. 6 correspond to the numbers in Table 2, identifying the solvent used. In contrast to PRODAN, an ASPD-doped multiphasic composite glass (data for 7 in Fig. 6) exhibits a much larger Stokes shift than expected from the macroaverage orientational polarizability of the matrix. In the current case, the dye was impregnated via an ethanol solution and deposited on the surface of the pores to form an interfacial phase. Therefore, we conclude that the microenvironment experienced by ASPD is a pure silica-like environment. Taking this assumption into account and using the orientational polarizability of pure silica, one obtains a better fit to the dependence exhibited by the solvent data, as shown by the data for 8 in Fig. 6. From the similarity in the behavior of the dye-doped sol–gel composite glass and dye–water solution, we conclude that in the composite glass the hydrogen bond donating effect is dominant, as it is in water,[44, 64] demonstrating that the dye is attached to the silica skeleton through hydrogen bonds.

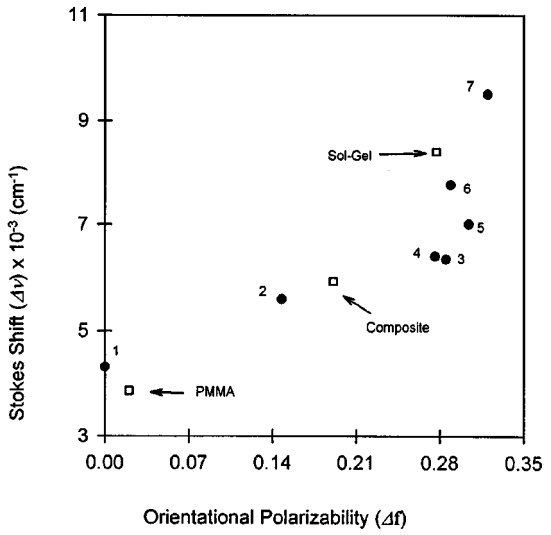

Figure 5 Lippert plot [Stokes shift (cm^{-1}) vs orientational polarizability (Δf)] for PRODAN. See text for details.

These two examples strongly support the claim of fabricating a multiphasic nanostructured composite glass,[24–26] since we are able to dope responsive materials either in the silica phase, interfacial phase or polymer phase. In each case,

Table 1 Spectral properties of PRODAN in varius solvents and solid matrices

No.	Solvent	E_x max. (nm)	E_m max. (nm)	$\Delta\tilde{\nu}$ (cm^{-1})	Δf [a]	n	ε
1	Cyclohexane	344	404	4317	0.000	1.424[b]	2.015[b]
2	Chloroform	355	443	5596	0.148	1.446[c]	4.806[c]
3	Acetone	350	450	6349	0.285	1.357[b]	20.7[b]
4	DMF	353	456	6399	0.276	1.427[b]	37.57[b]
5	Acetonitrile	349	462	7008	0.304	1.342[b]	33.59[b]
6	Ethanol	355	490	7761	0.289	1.359[b]	24.30[b]
7	Water	351	527	9515	0.320	1.332[b]	78.54[b]
8	PMMA	365	425	3868	0.020	1.496[d]	2.45[d]
9	Composite glass	354	448	5927	0.191	1.472[d]	7.8[d]
10	TMOS sol–gel	358	512	8401	~0.277	1.444[d]	~55[e]

[a] Orientational polarizability (Δf) is defined by Eqn [1] in the text.
[b] Data for refractive index (n) and dielectric constant (ε) at 25 °C are taken from Ref. 62.
[c] Data for refractive index (n) and dielectric constant (ε) at 20 °C are taken from Ref. 62.
[d] Data for refractive index (n) and dielectric constant (ε) are taken from Refs 5 and 10.
[e] Data are estimated following Refs 17 and 63.

the influence of the phase microenvironment on the spectroscopic properties of the dye should be taken into account.

2.4.2 Time-resolved fluorescence

Multifrequency phase and modulation fluorescence is a powerful technique for determining the excited-state decay kinetics of a fluorescent molecule. Figure 7 presents a typical multi-frequency data set for PRODAN-doped composite glass and their fits to various decay models.[38] The single-exponential fit in panel A is clearly poor and is confirmed by the residual plots in panels B and C. Table 3 collates the recovered lifetime(s) and the associated fractional intensities from the various decay models for PRODAN-doped composite glass (the data shown in Fig. 7). The quality of the fit of the various decay models can be compared by the recovered chi-squared $(\chi)^2$ value . A χ^2 close to unity indicates a good fit. A triple-exponential decay law is clearly a superior model for describing the experimental data. These results indicate that PRODAN is not in a homogeneous environment in the composite glass.

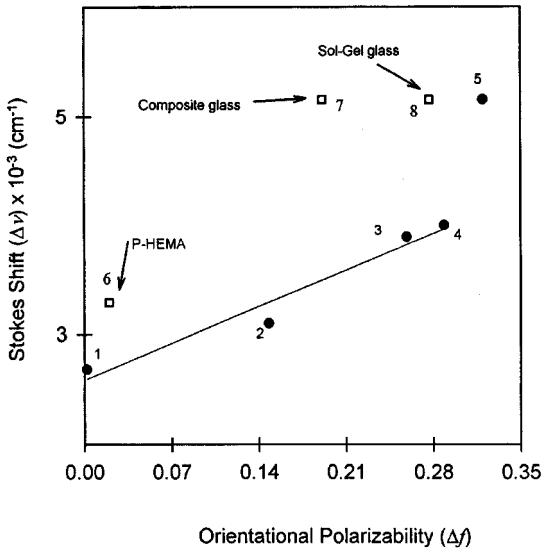

Figure 6 Lippert plot [Stokes shift (cm^{-1}) vs orientational polarizability (Δf)] for ASPT/ASPI. See text for details.

For the PRODAN-doped composite glass, a high contribution is due to a longer-lived component (τ=8.5 ns, 55%) with an additional shorter lifetime (τ=3.5 ns, 36%) resolved.[38] To obtain more insight into this system, we compared the recovered excited-state lifetimes for PRODAN doped in PMMA, composite glass and pure sol–gel (Table 3). From these comparisons we were able to conclude, first, that PRODAN experiences a heterogeneous microenvironment in the composite glass, PMMA and pure sol–gel; and second, that the recovered excited-state lifetimes for PRODAN doped in a composite glass are intermediate between those observed for pure PMMA and pure sol–gel, but more similar to those observed in pure PMMA. These results

Table 2 Spectral properties of ASPT in various solvents and solid matrices

No.	Solvent	A_b max. (nm)	E_m max. (nm)	$\Delta\tilde{\nu}$ (cm^{-1})	Δf [c]	n	ε
1	Benzene	486[a]	559[a]	2687	0.002		
2	Chloroform	483[a]	568[a]	3098	0.148	1.446[d]	4.806[d]
3	Cyclopentanone	490[a]	612[a]	3884	~0.259	1.437[e]	~17[g]
4	Ethanol	486[a]	603[a]	3992	0.289	1.359[e]	24.30[e]
5	Water	457[a]	598[a]	5159	0.320	1.332[e]	78.54[e]
6	Poly-HEMA[h]	485[b]	577[b]	3287	0.020	1.496[f]	2.45[f]
7	Composite glass	450	586	5157	0.191	1.472[f]	7.8[f]
8	Sol–gel glass	450	586	5157	~0.277	1.444[f]	~55[i]

[a] Data from Ref. 34.
[b] Data from Ref. 21.
[c] Orientational polarizability (Δf) is defined by Eqn [1] in the text.
[d] Data for refractive index (n) and dielectric constant (ε) at 20 °C are taken from Ref. 62.
[e] Data for refractive index (n) and dielectric constant (ε) at 25 °C are taken from Ref. 62.
[f] Data for refractive index (n) and dielectric constant (ε) are taken from Refs 5 and 30.
[g] Estimated following the value of cyclohexanone taken from Ref. 62.
[h] Was treated as PMMA.
[i] Data are estimated following Ref. 63.

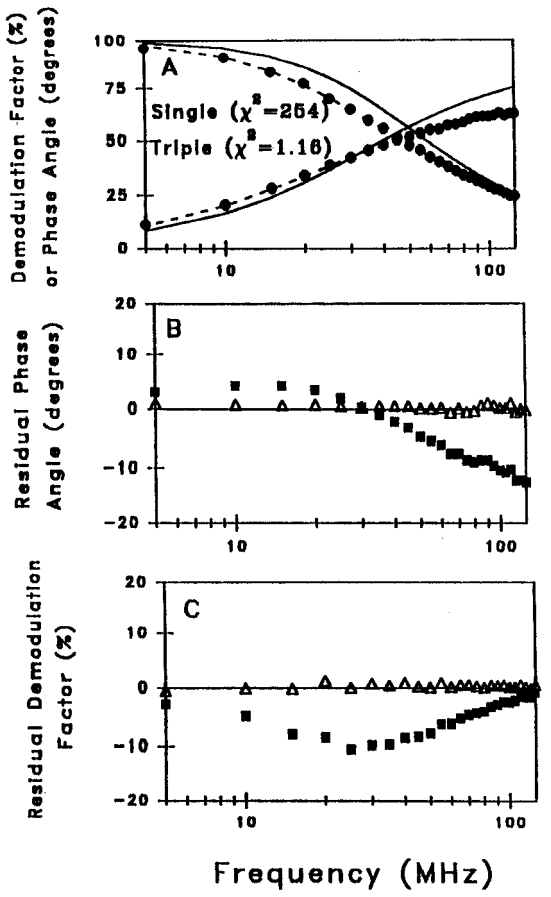

Figure 7 Typical multifrequency phase and modulation data for PRODAN-doped composite glass. (A) Phase angle and demodulation factor (●) and fits to various decay models [single-exponential (– – –) and triple-exponential (——) decay laws]. (B) Residual phase angle for fits to a single-exponential (■) and triple-exponential (△) model. (C) Residual demodulation factor for fits to a single-exponential (■) and triple-exponential (△) model.

Table 3 Recovered excited-state decay parameters for PRODAN-doped solid matrix using triple-exponential decay law

Matrix	τ_1^a (ns)	τ_2^a (ns)	τ_3^a (ns)	F_1^b	F_2^b
Composite glass	8.65	3.67	0.48	0.55	0.48
PMMA	13.4	3.85	0.65	0.36	0.56
TMOS sol–gel[c]	4.16	2.14	0.002	0.39	0.57

[a] Discrete lifetime.
[b] Fractional intensity.
[c] Data from Ref. 18.

support the steady-state results that PRODAN experiences a more PMMA-like environment in the composite glass. The PRODAN molecules which are located primarily in the PMMA phase are also influenced by the silica skeleton.

2.5 Organically doped, sol–gel-derived optical fibers

The ability to draw continuous fibers using the sol–gel process has been reviewed extensively by Sakka,[65] LaCourse[66] and Kamiya.[67] Under specific preparation conditions,[66, 68] fibers can be drawn by hand or a spinning apparatus up to 1 m in length. Recently,[27] we reported for the first time the preparation of micrometer-scale processed sol–gel-derived fibers doped with optically active organic dyes. The dye is doped in the precursor solution of the sol–gel process.

Briefly, a stock sol–gel solution was prepared by stepwise mixing of tetraethoxysilane, water, ethanol and hydrochloric acid in molar ratio of 1:1.5:1.9:0.01, respectively.[27] The ethanol solution used in the above step contained the dye to be entrapped within the sol–gel matrix. The dye-doped sol–gel solution was placed in a beaker, which was then sealed with aluminum foil and stored in an oven at 40 °C for gelation (several days). Just before gelation (indicated by the high viscosity of the sol–gel solution), sol–gel-derived, uniform, continuous fibers were drawn by hand or by a spinning apparatus. The fibers were kept for aging and drying under ambient conditions for a few weeks. In this way, fibers with diameters varying from 20 ± 3 to 200 ± 10 μm with a smooth surface were prepared.[27] The fibers were cut to a specific length without any polishing of the fiber ends. We observed an average attenuation loss of 60 dB m^{-1} from the organically doped sol–gel-derived fiber. However, each fiber includes several sections with losses as low as 10 dB m^{-1}.

We studied the potential of the dye-doped, sol–gel-derived optical fibers by doping them with fluorescein, a well-known pH-sensitive fluorescent probe,[71, 72] for chemical fiber sensing and with Rhodamine-6G, a well-known laser dye,[73] as a fiber laser medium. Figure 8 presents the emission spectra of R6G-doped and fluorescein-doped sol–gel-derived fibers. The fluorescence of dye-doped sol–gel-derived fiber[27] was measured on an SLM 48000 MHF spectrofluorimeter using a xenon arc lamp as the

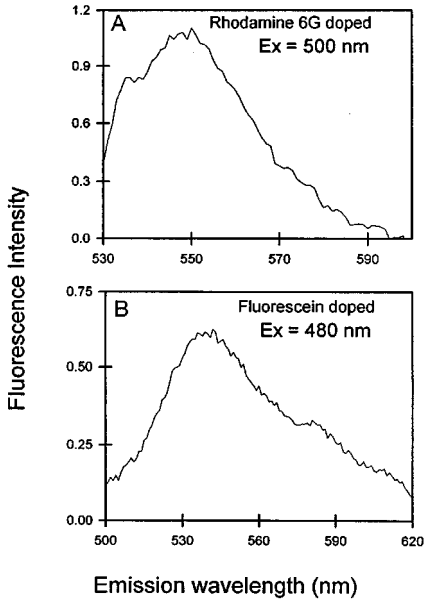

Figure 8 Fluorescence emission spectra of (A) 1 μM Rhodamine-6G-doped and (B) 1 μM fluorescein-doped within a sol–gel-derived optical fiber with a diameter of 20 ± 3 μm.

excitation source. Light from a 100 μm commercial optical fiber was coupled into the dye-doped sol–gel-derived fiber. The evanescent-wave emission was collected at 90° to the excitation. The resolution of the spectrofluorimeter is ±0.5 nm. The fluorescence spectrum was background-subtracted and corrected for detector and monochromator transmission nonlinearities. Extended discussions of these applications are presented in Section 4.

3 PHOTONIC APPPLICATIONS OF DOPED COMPOSITE GLASSES

3.1 Solid-state dye lasers

One of the most important applications of dye-doped solid matrices is the solid-state dye laser which makes it possible to achieve tunability in a solid-state device.[74] Until recently, liquid dye lasers were the main systems used to achieve tunability in the visible region. However, solid-state dye lasers have advantages over liquid dye lasers by being nonvolatile, nonflammable, nontoxic, compact and mechanically stable. The problem of heat dissipation; however, poses a serious impediment to their utilization in applications that require high powers under either continuous-wave (cw) or pulsed high-repetition-rate operation. In liquid dyes, on the other hand, a flowing solution or a jet is a practical means of solving the heat problem. In both cases photostability is a property of prime importance for selecting a laser dye.[75]

In recent years lasing from dye-doped solid matrices has been demonstrated by several groups via a one-photon excitation process[21, 22,76–80] and even via a two-photon excitation process.[45, 46] Excellent slope efficiencies (up to 39%) and lifetimes of sol–gel-processed solid-state dye lasers have been reported and it has been observed that ORMOSILs can exhibit longer lifetimes than in the solution state.[13] As was discussed previously, the advantage of a solid-state dye laser depends heavily on its photostability and mechanical properties. A sol–gel-derived composite glass is a promising matrix due to its high photostability,[40] optical quality, and mechanical stability compared with the other matrices considered.[11, 12, 39] Solid-state dye lasers are suitable for applications which require only low laser output, e.g. photodynamic therapy (PDT),[81, 82] medical diagnostics for tissues using laser-induced fluorescence (LIF)[83] and photodynamic purification of blood from viruses.[84]

In Sections 3.1.1 and 3.1.2 we review two current extended applications of a solid-state dye laser, (1) multi-excitation pumping (one- and two-photon excitation) of a dye-doped composite glass (the dye used was ASPD)[44–46] and (2) the multidye laser: a multiphasic nanostructure composite glass monolith containing two laser dyes, ASPD and R6G, in which the energy transfer between the two components is minimized to produce tunable laser output across the lasing region of both dyes.[26]

3.1.1 One- and two-photon pumped dye lasers

For lasing studies, ASPD, an ionic dye, was doped in the interfacial phase[44, 45] by placing the porous glass in an ASPD solution. After the glass had been completely impregnated by the solution it was removed from the solution and placed on a hotplate at ~45 °C for several hours until the solvent evaporated out of the glass leaving the dye on the surface of the pores. Then the pores were sealed by impregnating the glass in methyl methacrylate solution, which diffused into the

pores and polymerized *in situ*. The fabrication of the composite glass has been discussed in Section 2.

Lasing of ASPD in a composite glass by one-photon excitation pumping[44] was demonstrated in a cavity that consisted of a ~100% reflecting metallic back mirror, and a ~70% reflecting dielectric output coupler, which was in a transverse pump cavity configuration. The wavelength dependence of the ASPD–composite glass ($\sim 3.1 \times 10^{-3}$ M) laser output, under excitation with a frequency-doubled Nd:YAG laser, is presented in Fig. 9. The output peak is centered at ~593 nm with a full width at half-maximum (FWHM) of 2 nm. The dye laser spectrum was measured by passing the lasing output through a monochromator (SPEX Triplemate Model 1460) and collection on an optical multichannel analyzer (OMA-III, EG&G Princeton Applied Research). The spectrum is a collection of 11 pulses at a 1 Hz repetition rate.

The output energy vs input pump energy, under excitation with a frequency-doubled Nd:YAG laser (532 nm), is plotted in Fig. 10 for $\sim 3.1 \times 10^{-3}$ M ASPD in composite glass.[44] The lasing threshold observed was 0.244 mJ/pulse. A maximum lasing slope efficiency of ~9% in composite glass was observed under one-photon excitation. The laser output for the lasing slope efficiency measurements was measured with a United Detector Technology 350 linear/log optometer and each collected data point was an average of 10 pulses. From loss calculations, we obtained a good agreement between the total loss observed from the slope efficiency measurements and the sum of the losses which are due to the cavity (mirrors, diffraction and scattering losses). Therefore, we can conclude that there is no evidence for additional losses, such as excited-state absorption, which were observed for red perylimide dye-doped composite glass.[21, 40]

ASPD also exhibits a strong two-photon absorption at 1.06 μm followed by fluorescence in the red. By placing this laser media in an appropriate optical cavity and pumping it longitudinally with an intense IR beam, up-converted visible lasing was obtained. Lasing by two-photon excitation was first demonstrated in a polymer rod matrix[46] and, later, also in composite glass and composite Vycor glass.[45] However, contrary to the expectation that two-photon absorption is not an efficient process, the lasing energy conversion efficiency was found to be very high (~3.5%). For the polymer rod matrix, the lifetime in terms of pulse number was more than 4×10^4 pulses at 2 Hz repetition rate and under a pump energy of 1.3 mJ. Since it has been demonstrated that the photostability of a sol–gel/PMMA composite glass matrix is much higher than that of a polymer host (three orders of magnitude) under one-photon excitation,[40] we

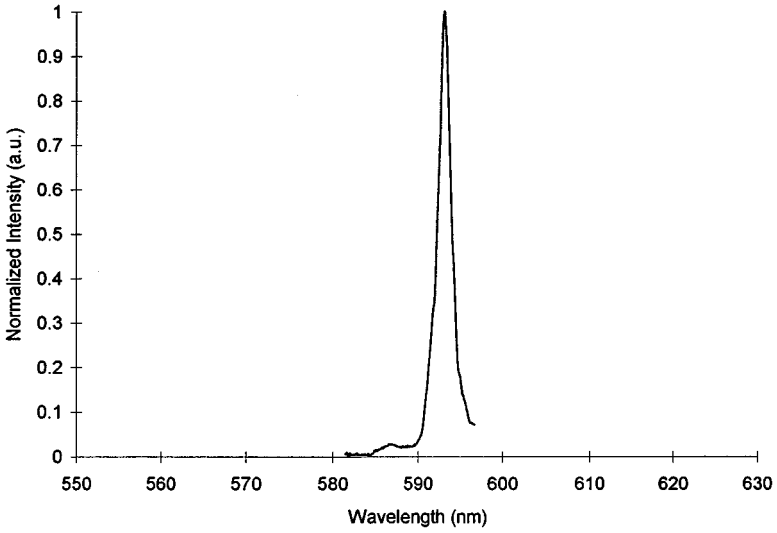

Figure 9 Lasing output intensity vs wavelength for ASPI composite glass. The composite glass was transverse pumped with a 8 ns pulsed frequency-doubled Nd:YAG laser at 532 nm operating at 1 Hz repetition rate, using a ~100% reflecting mirror as the back reflector.

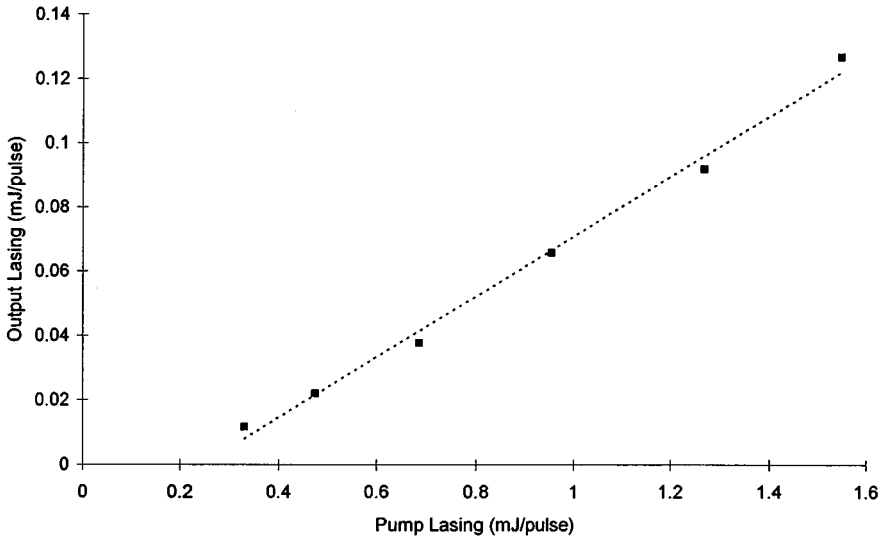

Figure 10 The output energy vs input pump energy, under excitation with a frequency-doubled Nd:YAG laser (532 nm) for ASPD in composite glass.

expect higher photostability in the glass-based matrices also under two-photon pumping. Up to now, these samples have been able to withstand an IR pump flux power of 400 MW cm^{-2} with 10 ns pulses without damage.[45, 46]

3.1.2 Multidye lasers

The multidye solid-state tunable laser consisted of ASPD, which resides in the interfacial phase, and R6G, which resides in the polymer phase.[26] The fabrication of a multiphasic composite glass is discussed in more detail in Section 2.2 and in Ref. 26. Tunable lasing was observed across the regions of the individual dyes. The laser output for tunability measurements was measured with a Jobin–Yvon UV Monochromator and a Si PIN photodiode. The photodiode output signal was measured with an oscilloscope (Tektronix 350 MHz, Model 2467). The wavelength was scanned manually and several measurements were made at each point.

Figure 11 presents the lasing tunability of a multiphasic composite glass containing both dyes. For reference, Fig. 11 also presents the lasing tunability of two composite glasses, containing each dye separately. Tunable narrow-band laser outputs were observed in a cavity consisting of a grating as the back reflector and a ~70% reflecting output coupler. The FWHM of the tunability spectra for the ASPD composite glass is ~21 nm and that for R6G ~12 nm. For the multiphasic composite containing both dyes it is ~37 nm. From these data it is evident that the glass containing both dyes is tunable across the range of both dyes (560–610 nm), whereas in the solution state the R6G emission is quenched.[26] We believe that the quenching in the solution state is a result of Förster energy transfer. Therefore, due to the extremely large ratio between the specific surface area and the pore volume, which is $\sim 8.5 \times 10^6$, it is possible to separate the two dye molecules (which reside in different phases) to a distance where the Förster energy transfer is no longer effective.

The rate of energy transfer between the donor molecule (Rhodamine-6G) and the acceptor molecule (ASPD) in the Förster energy-transfer mechanism can be described by Eqn [4]:[85]

$$k_T = \frac{9(\ln 10)\,\kappa^2 Q_d J}{128\pi^5 n^4 N_a \tau_d R^6} \qquad [4]$$

where κ^2 is the orientational factor for the dipole–dipole interaction, Q_d is the fluorescence quantum yield of the donor molecule without the acceptor molecule, n is the refractive index of the medium, N_a is Avogadro's number, τ_d is the fluorescence lifetime of the donor molecule in the absence of the acceptor, R is the distance between the centers of the donor and the acceptor molecules and J is the normalized spectral overlap integral. From Eqn [4] the rate of energy transfer is directly proportional to the orientational factor κ to the second power, and inversely proportional to the sixth power of the distance

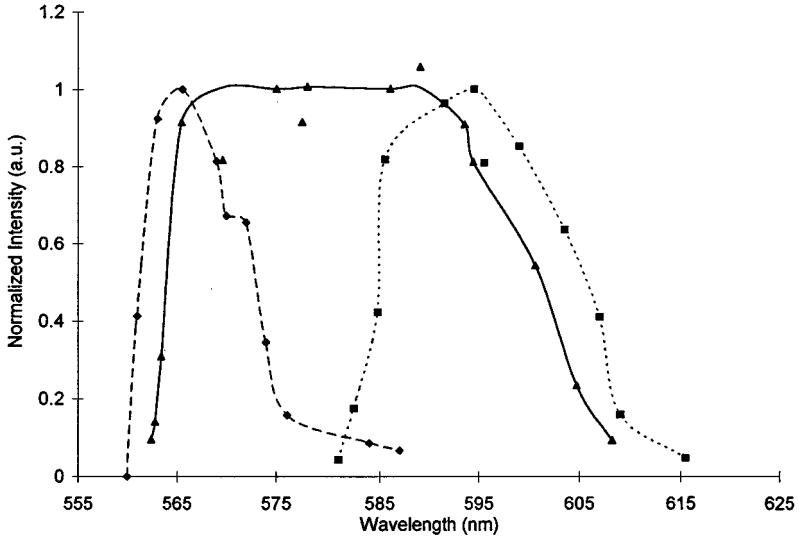

Figure 11 Lasing tunability of Rhodamine-6G composite glass (◆), ASPI composite glass (■), and the multiphasic composite glass containing both Rhodamine-6G and ASPI (▲). The composite glasses were transverse pumped with a 8 ns pulsed frequency-doubled Nd:YAG laser at 532 nm operating at a 1 Hz repetition rate, using a grating as the back reflector.

between the centers of the molecules. It is these two factors that we believe are significantly changed in the multiphasic composite glass. By increasing the distance between the molecules by a factor of 1.6 we have decreased the rate of energy transfer by more than one order of magnitude. Also, in the solution state, the molecules are free to rotate and sample most, if not all, of the orientational possibilities during the excited-state lifetime of Rhodamine-6G. In the solid state the molecules are effectively frozen in place with little or no rotation allowed, leading to a further decrease in the energy transfer.[26] Due to the change in the distance between the molecules and the decrease of the orientational factor, we have succeeded in preventing quenching due to Förster energy transfer (and other potential quenching mechanisms) in the multiphasic glass. We plan to pursue this type of study further to elucidate the unique properties of multiphasic nanostructured composite glasses relative to other materials in caging molecules in separate phases. This result represents the fascinating possibilities embodied in the multiphasic composite glasses for fabricating multifunctional devices for photonics.

3.2 Optical power limiters

Optical power limiters are devices which limit the optical output to a certain value. There are several physical mechanisms of optical power limiting action. e.g. nonlinear absorption, reverse saturable absorption, nonlinear refraction and thermal effects.[86] However, great success has recently been achieved in the design of optical power limitation using reverse saturable absorption mechanisms in phthalocyanines and their incorporation into sol–gel matrices.[87, 88] Each may be suitable for a specific condition. The multiphasic nanostructured composites may be specifically suitable for this purpose, because one can incorporate different power limiting functions in different phases. A good example of a multifunctional power limiting material is a monolith which contains C_{60} on the walls of the pores and BBTDOT in the polymer (PMMA) phase.[24, 25] C_{60} has shown optical power limiting behavior, which has been suggested to be due to a multitude of mechanisms such as reverse saturable absorption, nonlinear refraction and thermal effects;[86] BBTDOT shows a strong two-photon nonlinear absorption.[89]

The power limiting action of this multiphase composite was studied at two wavelengths: (1) at 532 nm, a wavelength where C_{60} is active due to reverse saturable absorption,[86, 90] and (2) at 800 nm, where the dye BBTDOT is active due to two-photon nonlinear absorption.[24, 89] The source at 532 nm was a frequency-doubled, Q-switched Nd:YAG laser which delivered 8 ns pulses at a repetition rate of 10 Hz. The source at 800 nm

was a dye laser with an IR dye (LSC 820) pumped at 532 nm which generated ~5 ns pulses at 800 nm. At each wavelength the transmitted intensity was recorded as a function of the incident intensity and the data were normalized to a transmissivity of unity at a low-intensity incident beam. An incident beam with pulse flux power up to 300 MW cm^{-2} was used in both cases. It is important to point out that the composites can stand up to 400 MW cm^{-2} pulse flux power.[24]

Figure 12 presents the normalized output fluence as a function of the input fluences for the multiphasic composite glass containing both C_{60} and BBTDOT, as well as for the two composite glasses containing each molecule separately.[24] From Fig. 12A, it is clear that C_{60} is more active as an optical limiter at 532 nm than at 800 nm, as expected from a one-photon induced reverse saturable absorption (RSA) process. BBTDOT has a linear absorption maximum at approximately 400 nm and, therefore, has almost no absorption in either 532 or 800 nm light at low intensity. This was supported by the measured transmissivity (at a low-intensity incident beam) of the pale yellow BBTDOT-doped sample, which was 0.98 at 800 nm and 0.70 at 532 nm. At higher intensities (>50 MW cm^{-2}) of the 800 nm beam, a strong two-photon absorption (TPA)-induced blue fluorescence was clearly visible in the sample. As expected (Fig. 12B), this glass shows a significantly higher nonlinearity at 800 nm than at 532 nm. On the other hand, the glass doped with C_{60} + BBTDOT had a light brown color and showed transmissivity (at a low-intensity incident beam) of 0.92 at 800 nm and 0.30 at 532 nm. The lower transmissivity at 532 nm is due to linear absorption of the C_{60} molecules. It can be clearly seen from Figure 12C that this sample shows excellent optical power limiting behavior at both 532 nm and 800 nm. The nonlinear behavior at 532 nm appears to be slightly enhanced compared with the sample doped with only C_{60}. This suggests that there may be a favorable contribution from BBTDOT. On the other hand, at 800 nm the nonlinearity is slightly less than that due to BBTDOT alone. This is probably attributable to the fact that the local intensity in the sample decreases due to the presence of C_{60} (some linear absorption). Therefore, the nonlinear absorption in BBTDOT, which varies as the square of the incident intensity, is reduced.

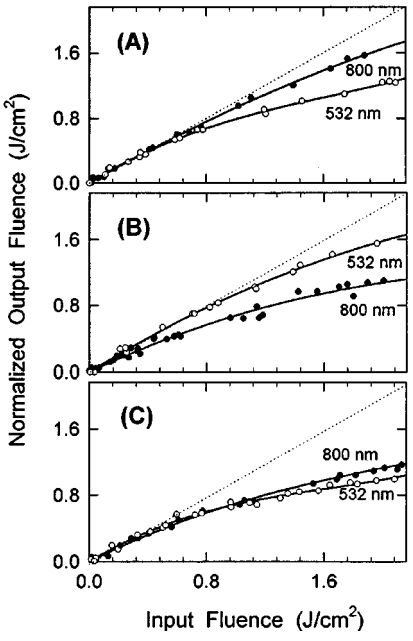

Figure 12 Normalized output fluence as a function of the input fluence for the three composite glasses at 532 nm (○) and 800 nm (●). (A) C_{60}-doped; (B) BBTDOT-doped; (C) C_{60} + BBTDOT-doped.

The multiphasic composite glass doped with both C_{60} and BBTDOT exhibited effective optical power limiting at both wavelengths, independently. The fact that we observed significant optical limitation using nanosecond pulses in the nanostructured composites is further evidence that in the multiphasic nanostructured composites the fullerene mimics its properties in solution, but is still phase-separated from the host material and other dopants. Therefore, this result represents another fascinating possibility embodied in multiphasic composite glasses, for fabricating multifunctional devices for photonics.

3.3 Nonlinear optical response

3.3.1 Nonlinear optics

Nonlinear optical processes provide key functions for photonics.[1–4] Examples of the nonlinear optical phenomena that are potentially useful include the ability to alter the frequency (or color) of light and to amplify one source of light with another, switch it, or alter its transmission characteristics through the medium, depending on its intensity. These processes can be viewed as dielectric phenomena and their origins can conveniently be explained by considering a

planar wave propagation through a nonlinear dielectric medium.[2] The polarization, *P*, induced in a dielectric medium by the incident optical field ($E_0 \cos \alpha$) can be written as:[3]

$$P = \chi^{(1)} E_0 \cos \alpha + \tfrac{1}{2}\chi^{(2)} E_0^2 (\cos 2\alpha + 1) + \chi^{(3)} E_0^3 (\tfrac{3}{4} \cos \alpha + \tfrac{1}{4} \cos 3\alpha) \quad [5]$$

The terms $\chi^{(n)}$ are bulk susceptibilities. The higher-frequency components (2α, 3α) appearing in Eqn [5] describe the nonlinear optical processes, examples being second-harmonic generation and third-harmonic generation. In addition, $\chi^{(3)}$ leads to the cos α term describing an intensity-dependent refractive index which gives rise to the Kerr effect, and leads to a mechanism for light control by light. Therefore, an intense beam can be used to change the refractive index of the medium and influence either its own propagation or the propagation of another beam having a different or the same frequency. The intensity dependence of the refractive index can also be used to generate a phase-conjugate signal in which the phase of a carrier wave is reversed to correct any frequency or phase distortions.

An effective third-order susceptibility $\chi^{(3)}$ can be calculated using degenerate four-wave mixing (DFWM) and homodyne optical Kerr gate (OKG) concentration dependence measurements.[91–93] In the concentration-dependent measurements, the intensity of the signal of the dye solution at zero time-delay is detected and compared with the intensity of the signal at zero time-delay of a reference; $\chi^{(3)}$ was calculated using Eqn [6].[93]

$$\chi^{(3)} = (n/n_{\text{ref}})^2 (I/I_{\text{ref}})^{1/2} (l_{\text{ref}}/l) \chi^{(3)}_{\text{ref}} F \quad [6]$$

where I stands for the DFWM/OKG signal intennsity, n is the refractive index of the medium, l is the interaction length, and the subscript ref refers to a reference sample; $\chi^{(3)}_{\text{ref}}$ is the third-order susceptibility of the reference. F is the correction factor taking into account the sample absorption. As there is no one-photon absorption for this dye at the wavelength of the measurements, only a two-photon absorption correction is necessary. For solution measurements, the effective $\chi^{(3)}$ calculated from Eqn [6] contains a contribution from both the solute and the solvent. Therefore, we treat the third-order susceptibility for the solution as a sum of two contributions,[93]

$$\chi^{(3)} = L^4 (N_s \gamma_s + N_x \gamma_x) \quad [7]$$

where γ_s and γ_x represent the second hyperpolarizabilities of the solvent and the solute, respectively. N_s and N_x denote the respective molecular densities, i.e. the number of molecules per cubic centimeters, and L is the local field correction factor approximated by the Lorentz expression

$$L = (n^2 + 2)/3 \quad [8]$$

where n is the refractive index of the solution at the frequency of the measurement (i.e. 602 nm or 620 nm). For each concentration, the effective $\chi^{(3)}$ value is calculated by using Eqn [6] and the γ values can be obtained by a least-squares fit to Eqn [7].

Molecules and polymers with π-conjugated electron systems show promising nonlinear optical properties.[5–8] Progress during the last decade in the design of organic molecules allows the preparation of new materials with high third-order optical susceptibility, for example heptamer dyes.[37, 43]

3.3.2 $\chi^{(3)}$ material-doped composite glass

We studied the nonlinear optical properties of two heptamer dyes, didecyl- and didecyloxy-substituted *p*-polyphenyl heptamers (DDPPH and DDOPPH, respectively) in composite glass, by conducting degenerate four-wave mixing and optical Kerr gate measurements.[43] In each measurement, a sample 1 mm thick was placed at the focus of the incident beams. Most of the instrumentation used for these measurements has been described previously.[91–93]

Figure 13(a) shows the time-resolved DFWM profile of DDPPH in a composite glass and Fig. 13(b) the time-resolved OKG profile of DDOPPH in a composite glass. The DFWM signal of DDPPH in the composite glass is narrower than the signal observed for this dye in solution and closer to the resolution provided by the pump pulse width. The sharpening of the fast signal allows us to observe a long decay signal (~0.8 ps). As reported previously,[92, 93] the third-order effect can be a combination of coherent instantaneous nonlinear response and a delayed part of the signal. The use of sub-picosecond pulses in the measurement makes it possible to separate the two components. One may envision two major processes responsible for the delayed component; the pump beam-induced reorientation of the molecules in the preferential direction of the pump polarization (molecular reorientation), and various nondirect processes due to the creation of excited states. Since we observed a

very strong UV–visible purple fluorescence from DDPPH under pumping at 620 nm, there is strong evidence that a two-photon absorption takes place within the power range used in our measurements. The presence of two-photon induced excited species is likely to contribute to the DFWM signal by the formation of a population grating with a slower decay rate compared with the coherent instantaneous signal. This DFWM signal derived from the two-photon excited population grating should depend on the fifth power of the input intensity, while the coherent instantaneous DFWM signal should reveal a third-power dependence on the intensity of the input beam.

In the case of the OKG signal of DDOPPH in the composite glass, the signal was broadened compared with the signal in the solution (Fig. 13b) without any significant long decay being observed.[43] The broadening could be a result of the heterogeneous microenvironment which the DDOPPH experiences in the composite, as was observed for PRODAN.[38]

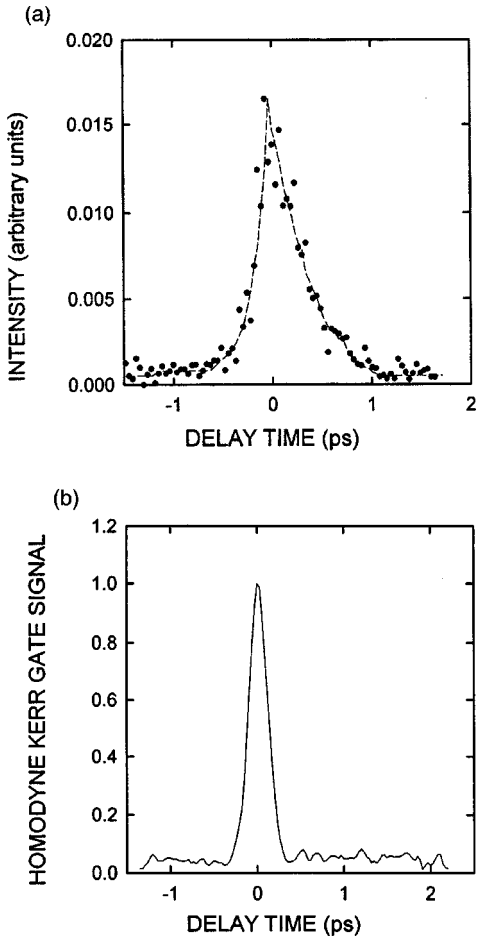

Figure 13 Temporal behaviour of (a) DFWM signal for DDPPH in a composite glass and (b) OKG signal for DDOPPH in a composite glass.

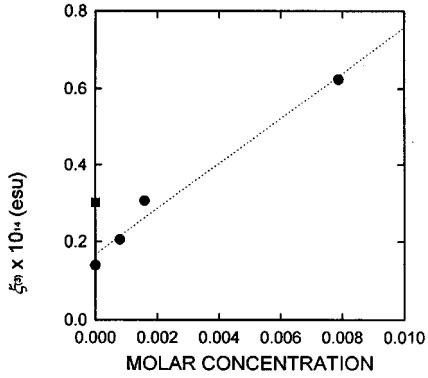

Figure 14 The concentration dependence of $\chi^{(3)}$ for DDPPH in a composite glass (●) measured using DFWM; ■, fused quartz microslide used as reference.

The concentration dependence of the effective $\chi^{(3)}$ of DDPPH in the composite glass, observed using DFWM measurements, is shown in Fig. 14. The intensity of the dye solution signal at zero time-delay is detected and compared with the intensity of the signal at zero time-delay of a reference.[43] Fused-quartz microslide glass was taken as a reference [$\chi^{(3)} = 0.3 \times 10^{-14}$ esu].[95] For each concentration, the effective $\chi^{(3)}$ value is calculated using Eqn [6] and the γ values can be obtained by a least-squares fit to Eqn [7]. The effective $\chi^{(3)}$ calculated from Eqn [6] contains a contribution from both the solute and the solvent, but, since the contribution from the matrix (composite glass) is considerably smaller, it can be negligible in this case. The concentration dependence of the effective $\chi^{(3)}$ for DDPPH in the composite glass, observed using DFWM measurements, is a linear function of the concentration. Therefore, only the absolute value (no sign) of γ real could be extracted using the least-squares fit to Eqn [7]. The lower γ value obtained in this measurement for DDPPH in the composite glass could indicate a lower two-photon absorption cross-section in the composite glass due to other competing processes, but this point warrants further investigation. The value of the effective $\chi^{(3)}$ achieved so far is limited since we have been unable to impregnate higher concentrations of the dye into the glass. In the composite glass, however, this lower nonlinearity can be compensated for by increasing the

interaction length. Although the results given above exhibit a limited nonlinearity performance, composite glass doped with heptamer dyes presents the ability to fabricate a solid-state nonlinear optical response in a monolith.

4 PHOTONIC APPLICATIONS OF ORGANICALLY DOPED, SOL–GEL-DERIVED OPTICAL FIBERS

4.1 Micron-scale chemical-sensing and biosensing fibers

Micrometer and submicrometer-scale fiber optical sensing was first demonstrated by Tan *et al*.[69, 70] Here, we demonstrate a micrometer-scale chemical-sensor and biosensor fiber application using a fluorescein-doped sol–gel-derived fiber where the fluorescein is doped in the sol–gel matrix. Fluorescein has been previously doped within sol–gel-derived monoliths and thin films as a pH-sensitive dye.[71, 72] The fluorescence quantum yield of fluorescein is pH-dependent, increasing with pH. We investigated the effect of pH on the fluorescence intensity by exposing the fluorescein-doped sol–gel-derived fiber (20 ± 3 μm) to ammonia and HCl vapors. Most of the instrumentation and the measurement set-up have been described in Section 2.5.

Figure 15(A) presents the percentage change (increase) in fluorescence intensity in the fluorescein-doped sol–gel-derived fiber upon

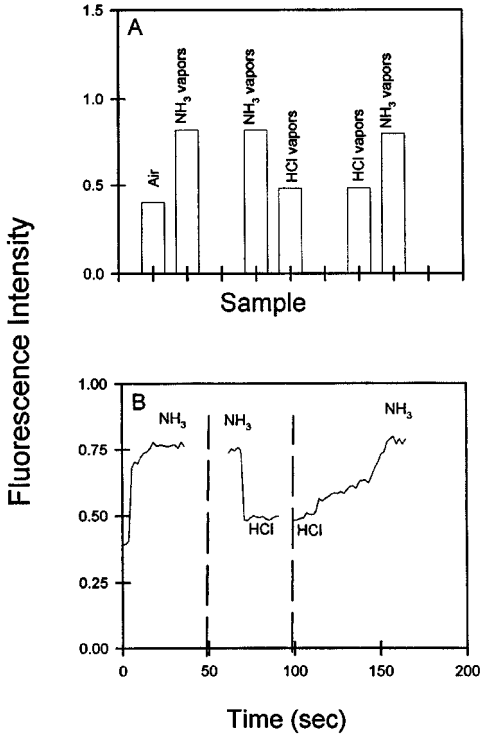

Figure 15 Percentage increase in fluorescence intensity in a fluorescein-doped sol–gel-derived fiber upon exposing the fiber to ammonia and HCl vapors.

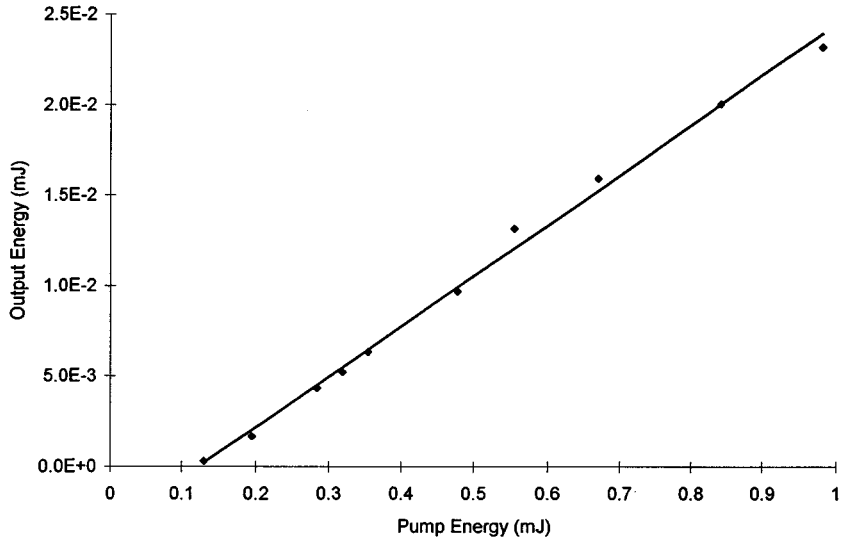

Figure 16 Lasing slope efficiency for Rhodamine-6G ($\sim 1 \times 10^{-4}$ M)-doped sol–gel fiber, 1 cm long, 150 μm thick, under pumping with an 8 ns pulsed frequency-doubled Nd:YAG laser at 532 nm operating at a 1 Hz repetition rate.

exposing the fiber to ammonia and HCl vapors.[27] A 50% increase in the fluorescence intensity was observed upon exposing the fluorescein-doped fiber to ammonia vapors. Upon exposing the same fiber to HCl vapors, there was a 45% decrease in the fluorescence intensity. These results clearly demonstrate that a fluorescein-doped sol–gel-derived fiber is sensitive to changes in pH. The response time of the fluorescein-doped sol–gel-derived fiber to ammonia and HCl vapors was observed to be 1–2 s (Fig. 15B). Upon further recycling, the response time increased by an order of magnitude. We believe that, in the experimental set-up described, there was strong adsorption of vapors by the doped optical fiber. Therefore, upon recycling the same fiber, the vapors first have to neutralize the adsorbed species, resulting in a longer response time. This is not a limitation of the sensor but of the present experimental set-up.

This method, with appropriate engineering, can be used to fabricate optical fiber-derived micrometer-scale sensors which can be easily used to detect environmental changes *in situ*. With a smaller fiber diameter (fibers of sub-micrometer dimension can be drawn under optimized conditions) an improved response time of the sensor is expected, as it has been achieved by Avnir and co-workers in the case of a pyranine-doped sol–gel-derived micropipette.[96] The advantages of our method are small dimensions for easy portability, no requirement for the use of lasers as the excitation source, excitation and emission via waveguide light, a long active path length, no tedious chemistry required to immobilize the active reagent, high photostability, high sensitivity and short response times.

4.2 Solid-state dye-doped fiber lasers

A solid-state dye-doped fiber laser application has been demonstrated using a R6G-doped sol–gel-derived fiber. R6G is a well-known laser dye which was chosen as the doped laser dye because of its very high lasing efficiency and solubility properties. Furthermore, this laser dye has been studied extensively.[73] One of the major drawbacks of Rhodamine-6G is its lack of photostability.[40, 97]

The system used for lasing performance studies of the fiber media was a frequency-doubled Quanta-Ray DCR Nd:YAG Q-switched laser with a repetition rate up to 30 Hz producing 8 ns pulses at 532 nm. The dye-doped fiber was longitudinally pumped and placed in a cavity consisting of a ~100% reflecting flat mirror (at 0°) and a ~70% reflecting flat output coupler (at 0° through the range 550–630 nm) at the two ends of the cavity. A more detailed description of the cavity design and measurement set-up is given elsewhere.[27] In this way, lasing performance was demonstrated. Amplication by a factor of 10 in the cavity lasing performance was demonstrated. Amplication by a factor of 10 in the cavity lasing compared with a single-pass super-radiance intensity (amplified emission under the conditions of a blocked back mirror) was achieved. The lasing intensity was extremely sensitive to the alignment of the cavity component due to the delicate coupling requirement into a micrometer-size fiber. Therefore we demonstrated the lasing with thick fibers (5.5 cm or 1 cm long, 150 μm in thickness).[28]

Figure 16 presents the relationship between measured dye output and pump input intensity for R6G ($\sim 1 \times 10^{-4}$ M)-doped sol–gel fiber (1 cm long, 150 μm thick) under pumping with a 8 ns pulsed frequency-doubled Nd:YAG laser at 532 nm operating at a 1 Hz repetition rate.[28] The pump beam and the lasing output were measured with a United Detector Technology 350 linear/log optometer and each data point collected was an average of 10 pulses. The lasing slope efficiency was calculated directly from the slope of the observed dye output–pump input intensity relationship. The observed slope efficiency was ~2.8%. A much higher slope efficiency is expected to be achieved by improving coupling into the fiber (by polishing the fiber ends), decreasing fiber optical loss, optimizing the concentration–length relationship (preventing aggregation effects) and improving the cavity desion in order to obtain a value closer to that observed for Rhodamine-6G in solution (>25%).[26]

This is the first report of a homogeneously dye-doped sol–gel-derived optical fiber operating as a laser medium. With appropriate improvements in preparation and laser design, this device can be fabricated and operated as a single-mode dye-doped fiber laser. By replacing the back mirror with a grating, tunable laser action is expected. We intend to extend our current studies to achieve this goal.

5 SUMMARY

We have demonstrated extended possibilities for a sol–gel matrix to develop new types of linear and nonlinear optical, organically doped materials. We have described methods of fabricating organically doped, multiphasic, nanostructured composite monoliths and organically doped, sol–gel–derived optical fibers. Examples of specific applications, such as a multidye solid-state tunable laser, a multiphasic optical power limiter, micrometer-scale chemical-sensing and biosensing fibers and a solid-state dye-doped fiber laser, have been discussed in detail.

Acknowledgements The authors are indebted to Ms Chen F. Zhao for synthesizing the aminostyrylpyridinium derivatives (APSD). We thank Dr J. D. Bhawalkar for providing us with his results of the optical power limiting measurements. We also thank Mr L. A. Baker for his diligent help in the preparation of the composite glasses and fibers. The current work was sponsored by the Air Force Office of Scientific Research and the Polymer Branch of Wright Laboratory through contact number F49620-93-C0017.

REFERENCES

1. B. E. A. Saleh and M. C. Teich, *Fundamentals of Photonics*, Wiley, New York, 1991.
2. Y. R. Shen, *The Principles of Nonlinear Optics*, Wiley, New York, 1984.
3. P. N. Prasad and D. J. Williams, *Introduction to Nonlinear Optical effects in Molecules and Polymers*, Wiley, New York, 1991.
4. D. S. Chemla and J. Zyss, *Nonlinear Optical Properties of Organic Molecules and Crystals*, Academic Press, Orlando, 1987.
5. R. Burzynski and P. N. Prasad, *Photonics and Nonlinear Optics with Sol–Gel Processed Inorganic Glass*: *Organic Polymer Composite*, Klein, L. C. (ed.), Kluwer Academic, Boston, 1994, Chapter 19.
6. P. N. Prasad, F. V. Bright, U. Narang, R. Wang, R. A. Dunbar, J. D. Jordan and R. Gvishi, in: *Hybrid Organic–Inorganic Composites*, Mark, J. E., Lee, C. and Bianoni, Y.–C. and P. A. (eds), American Chemical Society, ACS Symp. Ser. No. 585, Washington DC, 1995, Chapter 25.
7. P. N. Prasad and B. A. Reinhardt, *Chem. Mater.* **2**, 660 (1990).
8. D. M. Burland, R. D. Miler and C. A. Walsh, *Chem. Rev.* (1993).
9. H. L. and L. Gample, *Optics Comm.* **18**, 4 (1976).
10. E. J. A. Pope, M. Asami and J. D. Mackenzie, *J. Mater. Res.* **4**, 1018 (1989).
11. L. C. Klein, Nanocomposite fabrication for transparent windows, in: *Sol-Gel Optics*: *Processing and Applications*, Klein, L. C. (ed), Kluwer Academic Publishers, 1993; Chapter 10.
12. X. Li, T. A. King and F. Pallikari-Viras, *J. Non-Cryst. Solids* **170**, 243 (1994).
13. J. I. Zink and B. Dunn, in: *Sol–Gel Optics*: *Processing and Applications*, Klein, L. C. (ed), Kluwer Academic Publishers, Boston, 1993, Chapter 14.
14. D. Avnir, D. Levy and R. Reisfeld, *J. Phys. Chem.* **88**, 5956 (1984).
15. F. Salin, G. Le Saux, P. Georges, A. Brun, C. Bagnall and J. Zarzycki, *Optics Lett.* **14**, 785 (1989).
16. J. M. Mckiernan, S. A. Yamanaka, B. Dunn and J. I. Zink, *J. Phys. Chem.* **94**, 5652 (1990).
17. S. Braun, S. Rappoport, R. Zusman, D. Avnir and M. Ottolenghi, *Mater. Lett.* **10**, 1 (1990).
18. U. Narang, F. V. Bright and P. N. Prasad, *Appl. Spectrosc.* **47**, 229 (1993).
19. R. Gvishi and R. Reisfeld, *J. Non-Cryst. Solids* **128**, 69 (1991).
20. V. Chernyak, R. Reisfeld, R. Gvishi and D. Venezky, *Sensors and Materials* **2**, 117 (1990).
21. R. Gvishi, R. Reisfeld, Z. Burshtein and E. Miron, *SPIE Proc.* **1972**, 390 (1993).
22. R. Reisfeld, D. Brusilovsky, M. Eyal, E. Miron, Z. Burshtein and J. Ivri, *SPIE Proc.* **1182**, 230 (1989).
23. G. Puccetti, E. Toussaere, I. Ledoux and J. Zyss, *Polym. Prepr.* (*Am. Chem. Soc.*, *Div. Polym. Chem.*) **32**, 61 (1991).
24. R. Gvishi, J. Bhalwakar, D. N. Kumar, G. Ruland, U. Narang and P. N. Prasad, *Chem. Mater.* **7**, 2199 (1995).
25. P. N. Prasad, R. Gvishi, G. Ruland, D. N. Kumar, J. Bhalwakar and U. Narang, *SPIE Proc.* **2530**, 128 (1995).
26. G. Ruland, R. Gvishi and P. N. Prasad, *J. Am. Chem. Soc.* **118**, 2986 (1996).
27. U. Narang, R. Gvishi, F. V. Bright and P. N. Prasad, *J. Sol–Gel Sci. Tech.* in press (1995).
28. R. Gvishi, G. Ruland and P. N. Prasad, *Opt. Commun.* **126**, 66 (1996).
29. C. J. Brinker and G. W. Scherer, *Sol–Gel Science*, Academic Press, San Diego, 1990.
30. L. C. Klein (ed.) *Sol–Gel Technology For Thin Films*, *Preforms*, *Electronics*, *and Specialty Shapes*, Noyes, New Jersey, 1988.
31. L. C. Klein, *Sol–Gel Optics*: *Processing and Applications*, Kluwer Academic Publishers, Boston, 1993.
32. L. L. Hench and J. K. West, *Chem. Rev.* **90**, 61 (1990).
33. J. Livage, M. Henry and C. Sanchez, *Prog. Solid-State Chem.* **18**, 259 (1988).
34. H. Schmidt, *Mater. Res. Symp. Proc.* **171**, 3 (1990).
35. M. Yamane, in: *Sol–Gel Technology For Thin Films*, *Preforms*, *Electronics*, *and Specialty Shapes*, Klein, L. C. (ed), Noyes, New Jersey, 1988, Chapter 10.
36. L. L. Hench and J. L. Nogues, in: *Sol–Gel Optics*: *Processing and Applications*, Klein, L. C. (ed), Kluwer Academic Publishers, Boston, 1993, Chapter 3.
37. R. Gvishi, G. S. He, P. N. Prasad, U. Narang, M. Li, F.

V. Bright, B. A. Reinhardt and A. G. Dillard, *Appl. Spectrosc.* **49**, 82 (1995).
38. R. Gvishi, U. Narang, P. N. Prasad and F. V. Bright, *Chem. Mater.* in press (1995).
39. R. Gvishi, Ph.D. Thesis, The Hebrew University of Jerusalem, Jerusalem, Israel, 1993.
40. R. Gvishi, R. Reisfeld and Z. Burshtein, *J. Sol–Gel Sci. Tech.* **4**, 49 (1995).
41. G. S. He, R. Gvishi, P. N. Prasad, B. A. Reinhardt, J. C. Bhatt and A. G. Dillard, *Optics Commun.* in press (1995).
42. G. S. He, R. Gvishi, P. N. Prasad, B. A. Reinhardt, J. C. Bhatt and A. G. Dillard, *CLEO 95 Conference*, 1995, in press.
43. R. Gvishi, P. N. Prasad, B. A. Reinhardt and J. C. Bhatt, *J. Sol–Gel Sci. Tech.* Special Issue, 'Sol–gel preparation of nonlinear optical material' in press (1995).
44. C. F. Zhao, R. Gvishi, U. Narang, G. Ruland and P. N. Prasad, *J. Phys. Chem.* **100**, 4526 (1996).
45. C. F. Zhao, G. S. He, J. D. Bhawalkar, C. K. Park and P. N. Prasad, *Chem. Mater.* **7**, 1979 (1996).
46. G. S. He, J. D. Bhawalkar, C. F. Zhao and P. N. Prasad, *IEEE J. Quant. Electron.* **32**, 749 (1996).
47. J. Catalán and J. Elguero, *J. Am. Chem. Soc.* **115**, 9249 (1993).
48. U. Narang, R. Wang, P. N. Prasad and F. V. Bright, *J. Phys. Chem.* **98**, 17 (1994).
49. U. Narang, F. V. Bright and P. N. Prasad, *Appl. Spectrosc.* **47**, 229 (1993).
50. R. Wang, U. Narang, F. V. Bright and P. N. Prasad, *Anal. Chem.* **65**, 2671 (1993).
51. D. Levy and D. Avnir, *J. Phys. Chem.* **92**, 4734 (1988).
52. V. Kaufman, D. Avnir, D. Pines-Rojanski and D. Huppert, *J. Non-Cryst. Solids* **99**, 379 (1988).
53. J. M. McKiernan, S. A. Yamanaka, E. Knobbe, J. Pouxviel, S. Paraneh, B. Dunn and J. I. Zink, *J. Inorg. Org. Polym.* **1**, 87 (1991).
54. B. Dunn and J. I. Zink, *J. Mater. Chem.* **1**, 903 (1991).
55. J. R. Lakowicz, *Principles of Fluorescence Spectroscopy*, Plenum, New York, 1983, pp. 187–215.
56. Weber and Farris, *Biochemistry* **18**, 3075 (1979).
57. R. Gvishi and R. Reisfeld, *Chem. Phys. Lett.* **156**, 181 (1989).
58. P. Fromherz, *J. Phys. Chem.* **99**, 7188 (1995).
59. U. Narang, J. D. Jordan, F. B. Bright and P. N. Prasad, *J. Phys. Chem.* **98**, 8101 (1994).
60. F. Monte and D. Levy, *SPIE Proc. Sol–Gel Optics III* **2288**, 276 (1994).
61. L. Onsager, *J. Am. Chem. Soc.* **58**, 1488 (1936).
62. *CRC Handbook of Chemistry and Physics*, 71st edn, CRC Press, Boca Raton, FL, 1990.
63. D. Avnir, V. R. Kaufman and R. Reisfeld, *J. Non-Cryst. Solids* **74**, 395 (1985).
64. U. Narang, C. F. Zhao, F. V. Bright and P. N. Prasad, *J. Phys. Chem.* in press (1995).
65. S. Sakka, in: *Sol–Gel Technology For Thin Films, Preforms, Electronics, and Specialty Shapes*, Klein, L. C. (ed), Noyes, New Jersey, 1988, Chapter 7.
66. W. C. LaCourse, in: *Sol–Gel Technology For Thin Films, Preforms, Electronics and Specialty Shapes*, Klein, L. C. (ed.), Noyes, New Jersey, 1988, Chapter 9.
67. K. Kamiya, in: *Sol–Gel Optics: Processing and Applications*, Klein, L. C. (ed.), Kluwer Academic Publishers, 1993, Chapter 5.
68. W. C. LaCourse, S. Dabar and M. Akitar, *Commun. Am. Ceram. Soc.* **67**, C-200 (1984).
69. W. Tan, Z.-Y. Shi, S. Smith, Birnbaum and R. Kopelman, *Science* **258**, 778 (1992).
70. R. Kopelman, W. Tan and Z.-Y. Shi, *SPIE* **1796**, 157 (1993).
71. R. Reisfeld, M. Eyal and R. Gvishi, *Chem. Phys. Lett.* **138**, 377 (1987).
72. B. D. MacCraith, V. Ruddy, C. Potter, G. O'Keefe and J. F. McGilp, *Elect. Lett.* **27**, 1247 (1994).
73. K. H. Drexhage, in: *Dye Lasers*, Schäfer, F. P. (ed), Springer, Berlin, 1990, Chapter 5.
74. F. J. Durate, *Laser Focus World* **5**, 187 (1995).
75. R. Cunningham, *Laser Optron.* **2**, 30 (1991).
76. G. S. He, C. F. Zhao, C. K. Park, P. N. Prasad and R. Burzynski, *Opt. Commun.* **111**, 82 (1994).
77. B. Dunn and J. I. Zink, Sol–gel encapsulated molecules: optical probes and optical properties, in: *Sol–Gel Optics: Processing and Applications*, Klein, L. C. (ed.), Kluwer Academic Publishers, 1993, Chapter 14.
78. D. Lo, J. E. Parris and J. C. Lawless, *Appl. Phys. B* **56**, 385 (1993).
79. M. Canva, A. Dubois, P. Georges and A. Brun, *SPIE Proc.* **2288**, 298 (1994).
80. D. Shamrakov and R. Reisfeld, *Chem. Phys. Lett.* **213**, 47 (1993).
81. S. Andersson-Engles, J. Johansson, S. Svanberg and K. Svanberg, *Anal. Chem.* **61**, 1367 (1989).
82. T. J. Dougherty, *Photochem. Photobiol.* **45**, 879 (1987).
83. R. R. Alfano, D. B. Tata, J. Cordero, P. Tomashefsky, F. W. Longo and M. A. Alfano, *IEEE J. Quant. Elec.* **20**, 1567 (1984).
84. M. M. Judy, *Bio-laser News* **10**, 1 (1989).
85. M. R. Eftink, in: *Fluorescence Quenching: Theory and Application*, Lakowicz, J. R. (ed), *Topics in Fluorescence Spectroscopy*, Vol. 2, Plenum Press, New York, 1991, Chapter 2.
86. L. W. Tutt and T. F. Bogges, *Prog. Quant. Electron.* **17**, 299 (1993).
87. J. W. Perry, K. Mansour, S. R. Marder, C.-T. Chen, P. Miles, M. E. Kenny and G. Kwag, *Mater. Res. Soc. Symp. Proc.* **374**, 257 (1995).
88. P. D. Fuqa, B. Dunn and J. I. Zink, *SPIE Proc. Sol–Gel Optics III* **2288**, 239 (1994).
89. G. S. He, G. C. Xu, P. N. Prasad, B. A. Reinhardt, J. C. Bhatt and A. G. Dillard, *Opt. Lett.* **20**, 437 (1995).
90. B. L. Justus, Z. H. Kafafi and A. L. Huston, *Opt. Lett.* **18**, 1603 (1993).
91. Y. Pang, M. Samoc and P. N. Prasad, *J. Chem. Phys.* **94**, 5282 (1991).

92. M. E. Orczyc, M. Samoc, J. Swiatkiewicz and P. N. Prasad, *J. Chem. Phys.* **98**, 2524 (1993).
93. R. Gvishi, J. Swiatkiewicz, P. N. Prasad, B. A. Reinhardt and A. G. Dillard, *Nonlinear Optics* **12**, 107 (1995).
94. M. Zhao, Y. Cui, M. Samoc, P. N. Prasad, M. R. Unroe and B. A. Reinhardt, *J. Chem. Phys.* **95**, 3991 (1991).
95. I. Thomazeau, J. Etchepare, G. Grillon and A. Migus, *Opt. Lett.* **10**, 223 (1985).
96. J. Samuel, A. Strinkovski, S. Shalom, K. Lieberman, M. Ottolenghi, D. Avnir and A. Lewis, *Mater. Lett.* **21**, 431 (1994).
97. V. S. Antonov and K. L. Hola, *Appl. Phys. B* **32**, 9 (1983).